AGU PUBLICATIONS

JGR

Journal of Geophysical Research: Atmospheres

RESEARCH ARTICLE
10.1002/2014JD022363

Key Points:
- Turbulence effects on mixed-phase convective clouds are numerically examined
- Turbulence decreases precipitation from mixed-phase deep convective clouds
- Effects of turbulence are more pronounced in the uniform basic-state wind

Correspondence to:
J.-J. Baik,
jjbaik@snu.ac.kr

Citation:
Lee, H., J.-J. Baik, and J.-Y. Han (2014), Effects of turbulence on mixed-phase deep convective clouds under different basic-state winds and aerosol concentrations, *J. Geophys. Res. Atmos.*, *119*, 13,506–13,525, doi:10.1002/2014JD022363.

Received 29 JUL 2014
Accepted 13 NOV 2014
Accepted article online 18 NOV 2014
Published online 9 DEC 2014

Effects of turbulence on mixed-phase deep convective clouds under different basic-state winds and aerosol concentrations

Hyunho Lee[1], Jong-Jin Baik[1], and Ji-Young Han[2]

[1]School of Earth and Environmental Sciences, Seoul National University, Seoul, South Korea, [2]Korea Institute of Atmospheric Prediction Systems, Seoul, South Korea

Abstract The effects of turbulence-induced collision enhancement (TICE) on mixed-phase deep convective clouds are numerically investigated using a 2-D cloud model with bin microphysics for uniform and sheared basic-state wind profiles and different aerosol concentrations. Graupel particles account for the most of the cloud mass in all simulation cases. In the uniform basic-state wind cases, graupel particles with moderate sizes account for some of the total graupel mass in the cases with TICE, whereas graupel particles with large sizes account for almost all the total graupel mass in the cases without TICE. This is because the growth of ice crystals into small graupel particles is enhanced due to TICE. The changes in the size distributions of graupel particles due to TICE result in a decrease in the mass-averaged mean terminal velocity of graupel particles. Therefore, the downward flux of graupel mass, and thus the melting of graupel particles, is reduced due to TICE, leading to a decrease in the amount of surface precipitation. Moreover, under the low aerosol concentration, TICE increases the sublimation of ice particles, consequently playing a partial role in reducing the amount of surface precipitation. The effects of TICE are less pronounced in the sheared basic-state wind cases than in the uniform basic-state wind cases because the number of ice crystals is much smaller in the sheared basic-state wind cases than in the uniform basic-state wind cases. Thus, the size distributions of graupel particles in the cases with and without TICE show little difference.

1. Introduction

Turbulence is known to significantly affect the development of clouds by influencing various cloud microphysical processes, such as collision, diffusion of vapor, and mixing [*Grabowski and Wang*, 2013, and references therein]. Some studies have been tried to observe in-cloud turbulence structures [e.g., *Siebert et al.*, 2006, 2010]. However, because turbulent motions have spatial scales as small as a few millimeters, both numerical simulations and in situ observations that investigate the effects of turbulence on clouds and precipitation are hard to be realized till now. Therefore, attempts have been made to parameterize the effects of turbulence in numerical cloud models. Progress in this subject has been reported in *Khain et al.* [2007], *Devenish et al.* [2012], and *Grabowski and Wang* [2013].

Using direct numerical simulation (DNS) models [e.g., *Zhou et al.*, 2001; *Franklin et al.*, 2005; *Ayala et al.*, 2008; *Kunnen et al.*, 2013] and turbulence statistical models [e.g., *Pinsky et al.*, 2008], it has been shown that turbulence enhances the collision rate between small droplets up to several times compared to the gravitational collision rate. The enhanced collision can alter the development of clouds from the size distributions of cloud particles to surface precipitation. *Franklin* [2008] and *Riechelmann et al.* [2012] showed that droplets grow faster and raindrop formation is accelerated due to turbulence through the use of a DNS model and a Lagrangian cloud model coupled with a large-eddy simulation (LES) model, respectively. Using an LES model with bulk microphysics, *Seifert et al.* [2010] showed that the enhanced collision between small droplets increases surface precipitation in warm clouds. *Wyszogrodzki et al.* [2013], using an LES model with bin microphysics, also showed that surface precipitation in warm clouds increases due to turbulence under a specific range of aerosol concentrations.

While some previous studies have focused on the effects of turbulence on warm clouds, few studies have examined the effects of turbulence on mixed-phase clouds because of the complexity of these clouds. Some studies have shown that turbulence also enhances the rate of collision including ice particles [*Pinsky and Khain*, 1998; *Pinsky et al.*, 1998]. Using a 2-D cloud model with bin microphysics, *Benmoshe et al.* [2012] and

Benmoshe and Khain [2014] investigated the effects of turbulence on mixed-phase deep convective clouds with varying aerosol concentrations. *Benmoshe et al*. [2012] showed that the effects of turbulence decrease surface precipitation and are somewhat opposite to the effects of aerosol particles that increase surface precipitation from deep convective clouds. *Benmoshe and Khain* [2014] showed that the effects of turbulence on macrophysical properties of the mixed-phase clouds are comparatively small.

The aim of this study is to examine the effects of turbulence-induced collision enhancement on mixed-phase deep convective clouds under different basic-state winds and aerosol concentrations. Vertical wind shear has been appointed as one of the important factors that can regulate the evolution of deep convective clouds [e.g., *Weisman and Klemp*, 1982; *Thorpe et al*., 1982; *Rotunno et al*., 1988; *Fan et al*., 2009; *Han and Baik*, 2010]. Aerosol concentration is also known to affect the development of deep convective clouds. Some studies have been reported that increased aerosol number concentration can invigorate the development of deep convective clouds [e.g., *Rosenfeld et al*., 2008; *Lee et al*., 2010; *Han et al*., 2012; *Lee and Feingold*, 2013], while others have been reported aerosol number concentration that exceeds a certain threshold can suppress the development of deep convective clouds [e.g., *Seifert and Beheng*, 2006; *Fan et al*., 2009; *Carrió et al*., 2010; *Carrió and Cotton*, 2011]. For the purpose, this study adopts the 2-D cloud model with bin microphysics that was used in *Benmoshe and Khain* [2014]. The numerical model used in this study and the experimental setup are described in section 2. Simulation results are presented and discussed in section 3. A summary and conclusions are provided in section 4.

2. Model Description and Experimental Setup

The Hebrew University Cloud Model (HUCM) is used in this study. This is a 2-D cloud model that uses bin microphysics to treat the size distributions of hydrometeors. The model considers seven hydrometeor types [liquid water, three types of ice crystals (column, plate, and dendrite), snow, graupel, and hail]. To treat the size distribution of each hydrometeor type, the model uses 43 mass-doubling bins. The liquid fractions of snow, graupel, and hail are calculated at every model grid point and at every time step so that the time-dependent melting and freezing rates can be calculated more precisely. The rimed fraction of snow is calculated to estimate the density of snow particles more precisely. The density and terminal velocity of an ice particle depend on its radius, type, liquid fraction, and rimed fraction. Furthermore, if the density of snow whose radius is larger than 0.6 mm is larger than 200 kg m^{-3}, the snow particle is converted into the graupel particle, and if the rimed fraction of snow whose radius is smaller than 0.6 mm is larger than 0.95, the snow particle is converted into the hail particle. Detailed descriptions of the model are given in *Khain et al*. [2011].

It might be arguable to use a 2-D model to investigate the vertical wind shear effects or the turbulence effects. However, it is not impossible to use a 2-D model to investigate the effects. Some literatures have shown that 2-D models can be used under restricted conditions. For example, *Rotunno et al*. [1988] showed that the essential physics of clouds with one-directional vertical wind shear is contained in the 2-D framework. *Fan et al*. [2009] demonstrated that the wind shear effects on regulating the aerosol effects on isolated deep convective clouds in 2-D simulations are basically the same as those in 3-D simulations. *Benmoshe et al*. [2012], which used the same cloud model as in this study, gave a detailed description on the capability of the 2-D model to describe 3-D convective and turbulent motions and showed that the model can reproduce velocity statistics close to those of 3-D turbulence. We believe that the 2-D cloud model used in this study is also capable of investigating the turbulence effects on deep convective clouds with or without one-directional vertical wind shear.

According to previous studies [e.g., *Pinsky et al*., 1998; *Ayala et al*., 2008; *Pinsky et al*., 2008; *Grabowski and Wang*, 2013], turbulence increases the collision rates between cloud particles. This is because turbulence induces (1) the relative fluctuation motion of cloud particles via local shear and acceleration of a flow (i.e., an increase in swept volume), (2) the preferential distribution of cloud particles, and (3) an increase in collision efficiencies. To consider turbulence-induced collision enhancement (hereafter, TICE) on drop-drop collisions and drop-graupel collisions, the results of *Pinsky et al*. [2008] and *Pinsky et al*. [1998], which were obtained using turbulence statistical models, have been applied, respectively. *Pinsky et al*. [2008] considered all the above three mechanisms to calculate TICE between drop-drop collisions, and *Pinsky et al*. [1998] considered only the swept volume mechanism to calculate TICE between drop-graupel collisions. One advantage of the turbulence statistical models compared to DNS models [e.g., *Ayala et al*., 2008] is that the models can be applied to relatively high Taylor microscale Reynolds numbers (up to 20000). Detailed comparisons of the

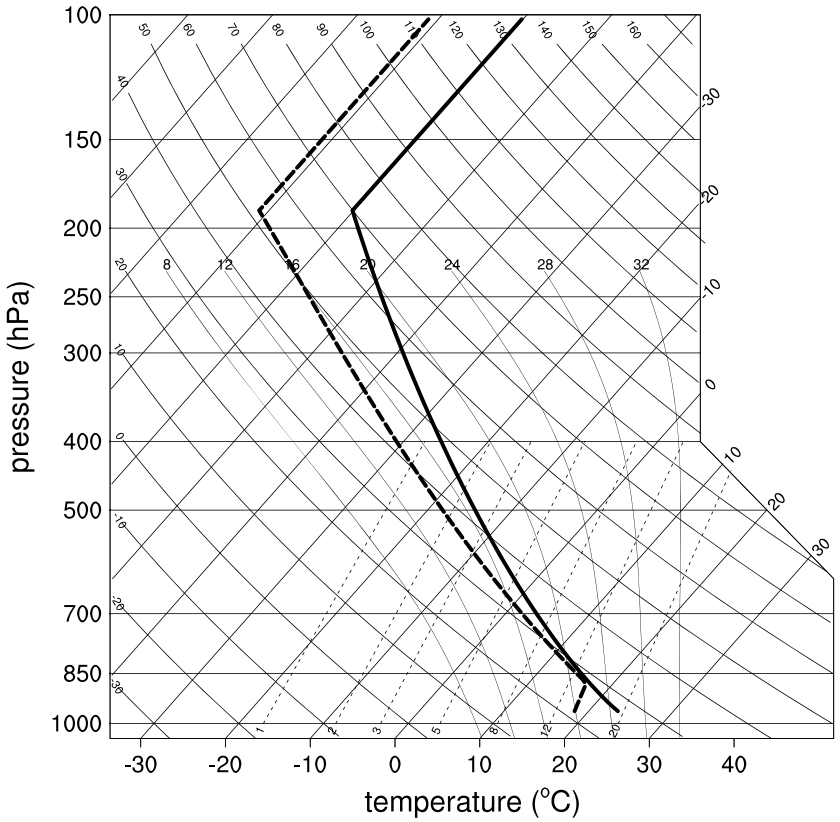

Figure 1. Thermodynamic sounding used in this study, which is adopted from *Weisman and Klemp* [1982]. Thick solid and dashed lines indicate the air temperature and dew point temperature, respectively.

turbulence statistical models used in these studies and DNS models are given in *Grabowski and Wang* [2013]. Unlike *Benmoshe and Khain* [2014], this study apply TICE only to drop-drop collisions and drop-graupel collisions because the turbulent flows near ice crystals or snow aggregates, which have very irregular shapes, are highly uncertain.

TICE is determined by the turbulence dissipation rate and the Taylor microscale Reynolds number that are diagnostically calculated using the turbulent kinetic energy. The cloud model predicts the turbulent kinetic energy using the 1.5th order turbulence closure. $L/15$, where L is the linear cloud size of the simulated cloud, is used as an external turbulence scale to calculate the turbulent kinetic energy in the cloud. For the details on calculating the turbulent parameters, see *Benmoshe et al*. [2012].

To simulate mixed-phase deep convective clouds, the thermodynamic sounding used in *Weisman and Klemp* [1982] is adopted (Figure 1). Two basic-state wind profiles are used: one is expressed by a tangent hyperbolic function $U = U_s \tanh(z/z_s)$ with $U_s = 15\ \mathrm{m\ s^{-1}}$ and $z_s = 3\ \mathrm{km}$, while the other is a uniform wind with a speed of $3\ \mathrm{m\ s^{-1}}$. In this study, for simplicity, all aerosol particles are assumed to serve as cloud condensation nuclei (CCN) according to supersaturation and aerosol particle size. Following *Khain et al*. [2000], the initial aerosol size distribution is determined using the Twomey equation [*Twomey*, 1959] and the

Table 1. Names and Settings of Eight Simulations Performed for This Study

	Collision Kernel	Basic-State Wind	CCN Concentration at 1% of Supersaturation ($\mathrm{cm^{-3}}$)
TU500	turbulence	uniform	500
GU500	gravitation	uniform	500
TU4000	turbulence	uniform	4000
GU4000	gravitation	uniform	4000
TS500	turbulence	sheared	500
GS500	gravitation	sheared	500
TS4000	turbulence	sheared	4000
GS4000	gravitation	sheared	4000

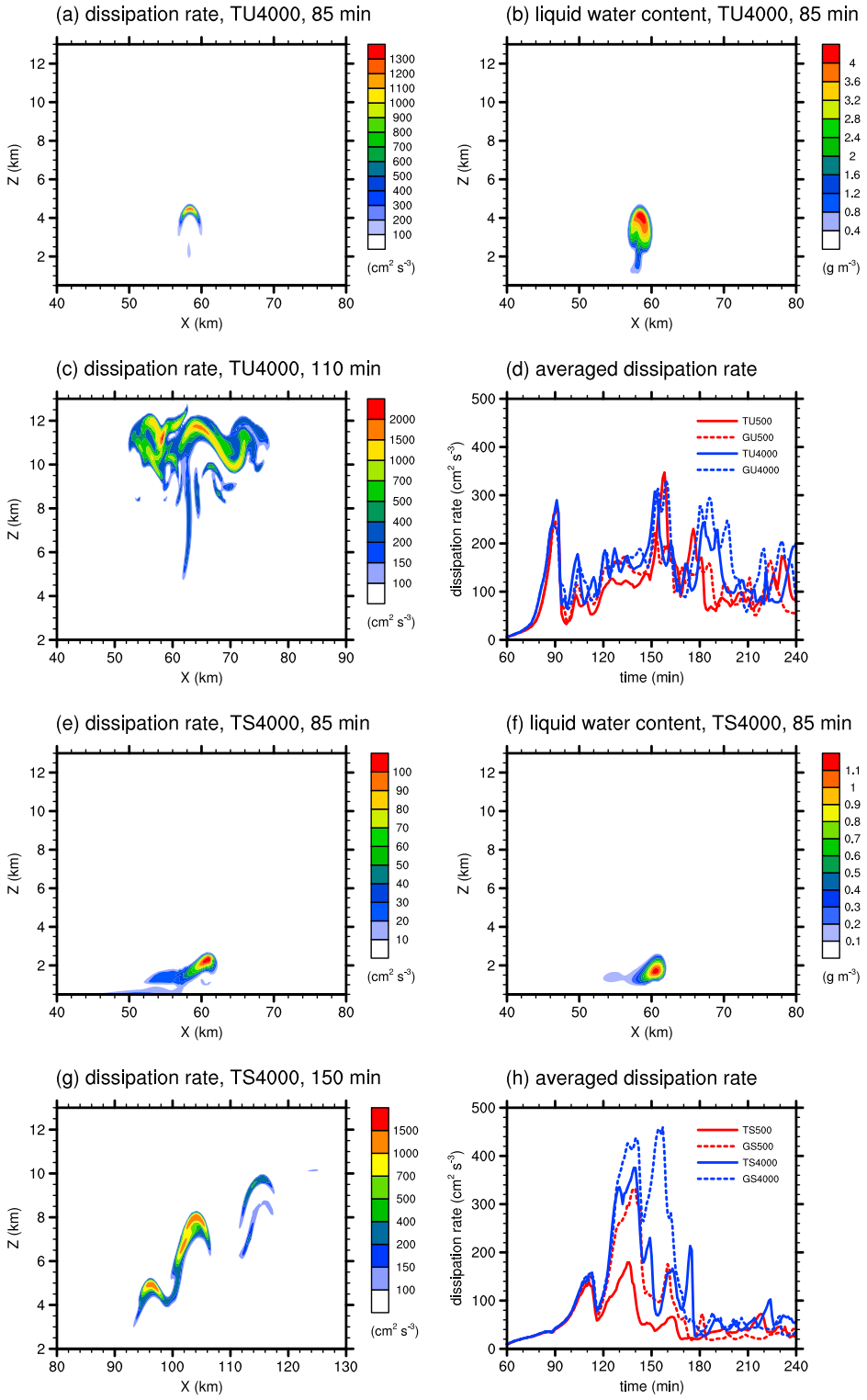

Figure 2. (a) Turbulence dissipation rate field at $t = 85$ min, (b) liquid water content field at $t = 85$ min, (c) turbulence dissipation rate field at $t = 110$ min in TU4000, and (d) the mean turbulence dissipation rate time series averaged over cloud area (drop number concentration is larger than 10 cm^{-3}) in the uniform basic-state wind cases. (e–g) The same as Figures 2a–2c, but for TS4000. (h) The same as Figure 2d, but in the sheared basic-state wind cases.

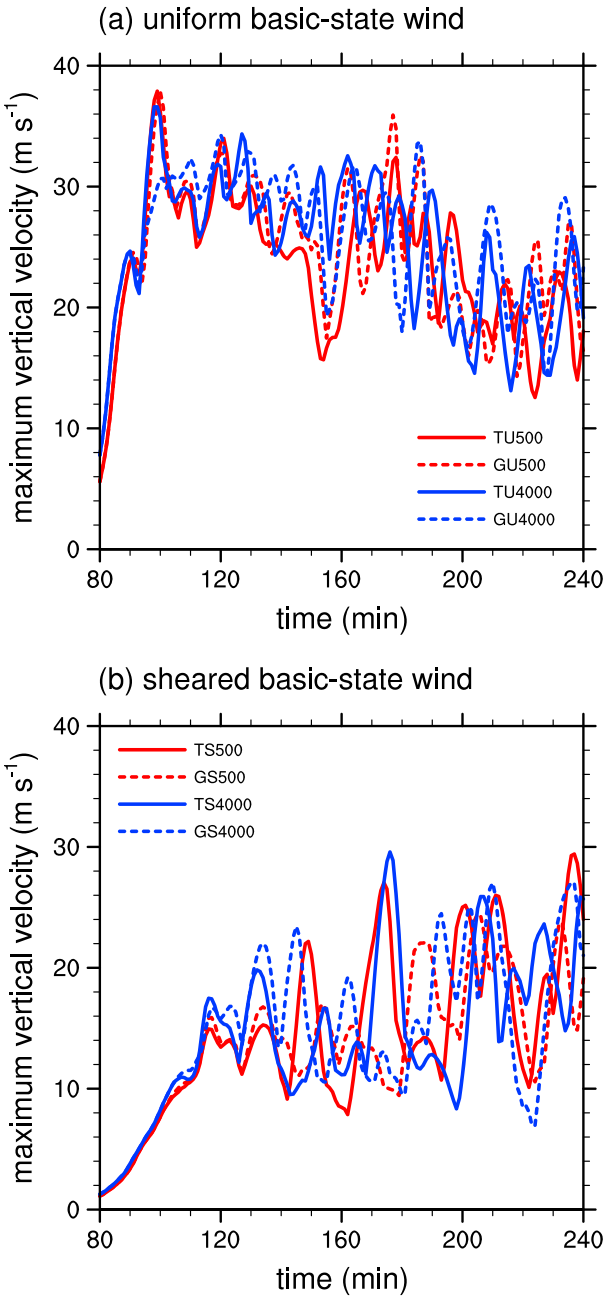

Figure 3. Maximum vertical velocity time series in (a) the uniform basic-state wind cases and (b) the sheared basic-state wind cases.

Köhler equation [*Köhler*, 1936]. The aerosol size distribution $N(r_a)$ is expressed by

$$\frac{dN}{d\ln r_a} = \frac{3}{2} N_0 k \left(\frac{4A^3}{27Br_a^3}\right)^{k/2}, \qquad (1)$$

where r_a is the radius of aerosol, N_0 is the CCN concentration at 1% supersaturation, k is a constant, A is a temperature-dependent coefficient that is related to the curvature effect, and B is a constant that is related to the solution effect. The value of k is specified as 0.5. To examine the effects of TICE with different aerosol concentrations, 500 cm^{-3} and 4000 cm^{-3} are used for N_0, which are in a typical aerosol concentration range used in studies on continental deep convective cloud simulations [e.g., *Carrió et al.*, 2010; *Han et al.*, 2012; *Benmoshe and Khain*, 2014]. To consider the formation of ice nuclei in the model, deposition and condensation-freezing nucleation in *Meyers et al.* [1992], immersion freezing in *Bigg* [1953] and *Vali* [1975], and secondary ice crystal formation in *Hallett and Mossop* [1974] are included.

Table 1 lists the names and settings of the eight simulations performed for this study. The domain size is 256 km in the horizontal and 18 km in the vertical. A damping layer is included from $z = 14$ km to the model top height. The grid size is 250 m in the horizontal and 125 m in the vertical. The time step is 4 s except for the diffusional process (0.4 s), and the integration time is 4 h. Convection is initiated by the specified low-level heating, whose half-width is 10 km, *e*-folding depth is 350 m, strength is 6×10^{-4} K s^{-1}, and duration is 100 s.

3. Results and Discussion

3.1. Cloud Structures

Figure 2 shows the turbulence dissipation rate and cloud water content fields in TU4000 and TS4000 and the averaged turbulence dissipation rate time series for all simulation cases. At the early cloud development stage, the highly turbulent zones and the drop-concentrated zones are generally collocated near the cloud top (Figures 2a, 2b, 2e, and 2f). This also commonly appears in previous studies [e.g., *Seifert et al.*, 2010; *Benmoshe et al.*, 2012], demonstrating that the strong turbulence effectively affects collisions between small droplets at the early cloud development stage.

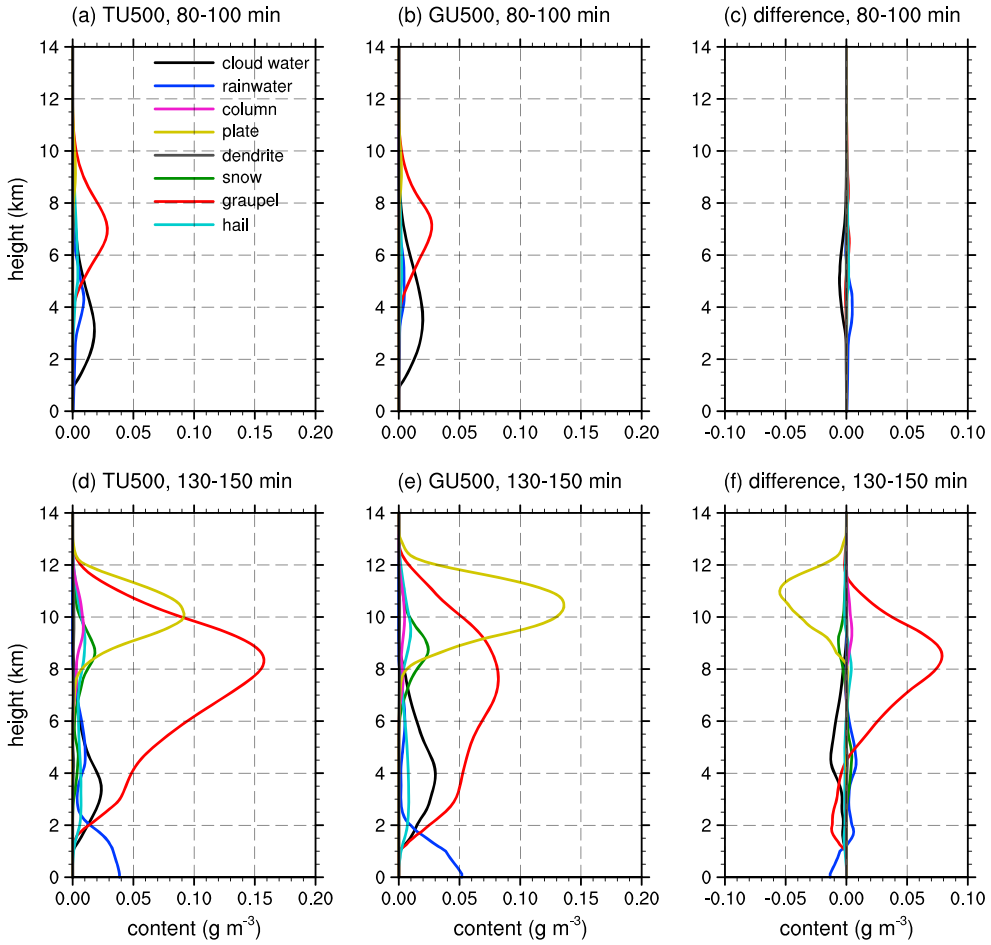

Figure 4. Vertical distribution of horizontally averaged mass of each hydrometeor type averaged for $t = 80–100$ min in (a) TU500 and (b) GU500. (c) The difference between Figure 4a and 4b. (d–f) The same as Figures 4a–4c, but averaged for $t = 130–150$ min.

At the mature stage of cloud development (Figures 2c and 2g), a few bubbles are shown in the clouds, and the typical size of the bubbles is order of a few kilometers, which are approximately 10–20 times of the model grid size. Compared to the results in *Benmoshe and Khain* [2014], the number of bubbles in the clouds is small and the typical size of bubbles is large in this study. These results might be due to the coarser grid resolution used in this study (250 m in this study, while 50 m in *Benmoshe and Khain* [2014]). However, although it might be possible that the coarser grid resolution decreases turbulence intensity due to the decreased intensities of local wind shear and buoyancy, the overall range of the simulated maximum turbulence dissipation rates is similar in both studies (approximately 1000–2500 $cm^2\ s^{-3}$). Moreover, the averaged turbulence dissipation rate time series in both studies also show similar intensities (Figures 2d and 2h). Therefore, it can be concluded that the grid size in this study is suitable if focus is on the examination of the effects of turbulence on collisions of cloud particles and the resultant changes in cloud development.

The background vertical wind shear and the CCN concentration affect the intensity and the spatial distribution of turbulence dissipation rate. In the sheared basic-state wind cases, high turbulence dissipation rates are maintained during relatively shorter periods. For example, the turbulence dissipation rates are higher than ~100 $cm^2\ s^{-3}$ for less than 60 min, whereas the rates are almost always maintained to be higher than ~100 $cm^2\ s^{-3}$ in the uniform basic-state wind cases (Figures 2d and 2h). Moreover, high turbulence dissipation rates tend to be concentrated near the cloud top in the uniform basic-state wind cases, whereas the high rates tend to be elongated and are distributed across relatively wider areas in the sheared basic-state wind cases (Figures 2c and 2g). It is also seen that the higher CCN concentration generally

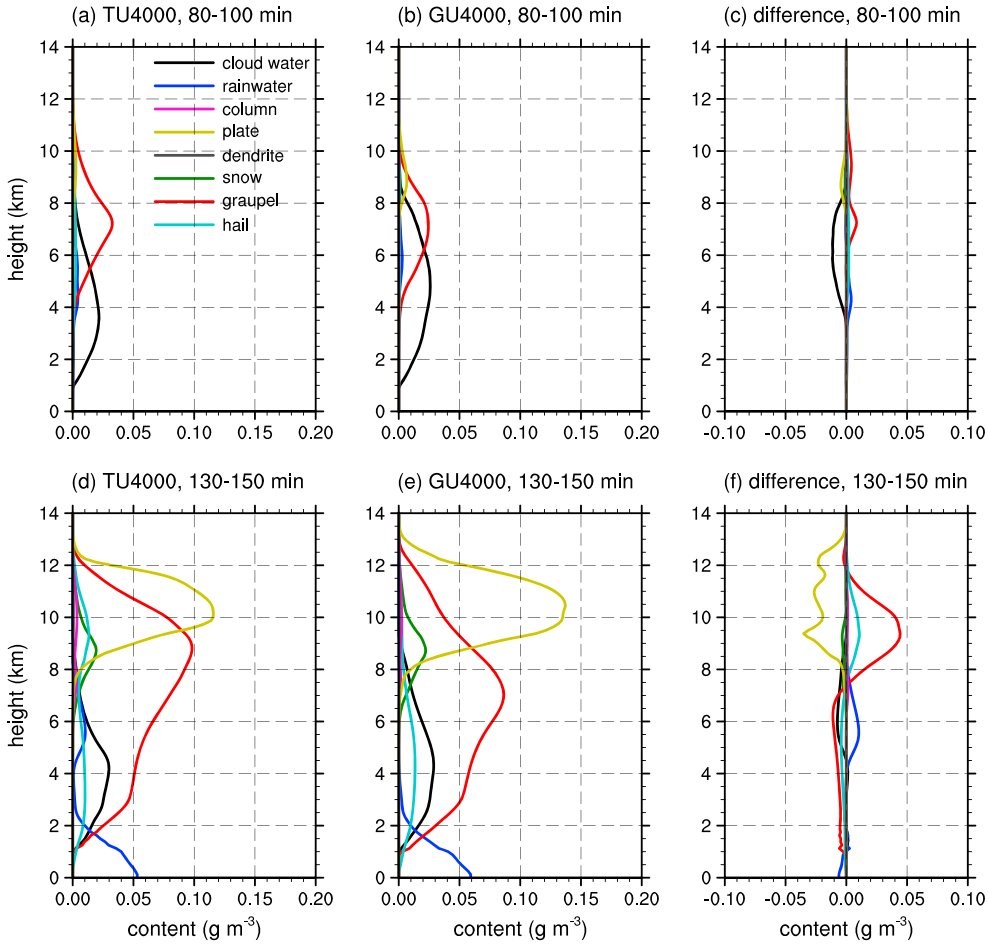

Figure 5. The same as Figure 4, but for TU4000 and GU4000.

tends to induce higher turbulence dissipation rates in the clouds (Figures 2d and 2h). This also appears in *Benmoshe and Khain* [2014], which mainly results from more condensational heat release due to the higher CCN concentration.

Figure 3 depicts the maximum vertical velocity time series. The series generally agree with the results in *Weisman and Klemp* [1982]: the maximum vertical velocity reaches to a relatively high value (~40 m s^{-1}) and tends to decrease with time in the uniform basic-state wind cases, while the secondary convection also has intensities similar to those of the initial convection in the sheared basic-state wind cases. The effects of CCN concentration on the maximum vertical velocity are not clear as a whole. In this study, the maximum vertical velocity is mainly determined by the instability of thermodynamic sounding and the basic-state wind shear, while the increased CCN concentration affects only local vertical motions. The cloud top height also is more likely affected by the basic-state wind shear, and the effects of the increased CCN concentration on the cloud top height are limited, which will be shown in the following sections.

3.2. Microphysical Structures in the Uniform Basic-State Wind Cases

The vertical distribution of temporally and horizontally averaged mass of each hydrometeor type for the uniform basic-state wind cases are depicted in Figures 4 and 5. Figure 4 is for TU500 and GU500, while Figure 5 is for TU4000 and GU4000. When $t = 80–100$ min, the effects of TICE appear to be similar regardless of the CCN concentrations. Although the differences are small, TICE induces a decrease in cloud water mass and an increase in rainwater mass. This is simply due to the accelerated coalescence between small droplets. During this period, almost all ice particles consist of graupel particles, and TICE increases graupel mass. TICE causes the produced graupel particles to grow more quickly because of the enhanced collision between

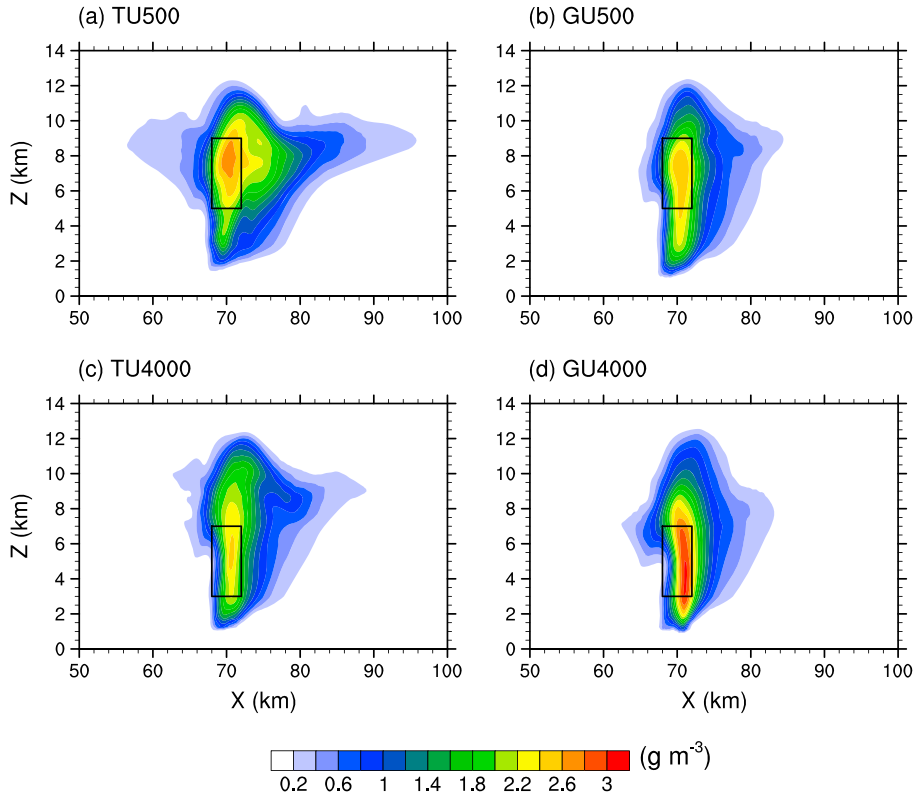

Figure 6. Graupel mass fields averaged for $t = 130–150$ min in (a) TU500, (b) GU500, (c) TU4000, and (d) GU4000. The rectangular box indicates the cloud core area.

graupel particles and droplets. Hail mass also increases due to TICE, but the differences are small. These changes are more pronounced for the high CCN concentration than for the low CCN concentration.

When $t = 130–150$ min, the main differences in the vertical mass distribution induced by TICE commonly appear under both the low and the high CCN concentration. Cloud water mass in TU500 and TU4000 is still smaller than that in GU500 and GU4000, respectively. During this period, it is seen that most of the cloud mass consists of ice particles, in particular plate-type ice crystals and graupel particles. Most of the ice crystals, which are mainly plate-type ice crystals, are present in the layer $z > 8$ km. Due to TICE, plate-type ice crystal mass decreases and graupel mass in the upper layer ($z > 5$ km in TU500 and GU500 and $z > 7$ km in TU4000 and GU4000) increases. This shows that the growth from ice crystals to graupel particles becomes more rapid due to TICE. When TICE is considered, however, graupel mass in the lower layer and rainwater mass in the layer $z < 1$ km decrease. The amount of surface precipitation (rainwater mass at the surface) is then reduced due to TICE during this period.

Previous studies have shown that surface precipitation from mixed-phase deep convective clouds is mainly contributed by the melting of ice particles, in particular when the freezing level is relatively low [e.g., *Khain et al.*, 2011]. Figures 4f and 5f also seem to suggest that it is the decrease in graupel mass in the lower layer that leads to the decrease in surface precipitation. This is examined with the graupel mass field averaged for $t = 130–150$ min (Figure 6). For both the low and the high CCN concentration, graupel particles in the upper layer ($z > 8$ km) are distributed more widely when TICE is included. However, graupel mass along the narrow shaft area in the lower layer ($x \sim 70$ km and $z < 6$ km) is reduced due to TICE. This decrease in graupel mass in the lower layer is consistent with the results shown in Figures 4 and 5.

Figure 7 shows the size distribution of graupel particles in the cloud core area in TU500, GU500, TU4000, and GU4000. In the number size distribution, the radii of most graupel particles range between 10 μm and 1 mm. The number concentration of graupel particles whose radii are larger than ~300 μm increases due to TICE. Also, the number-averaged graupel particle radius increases due to TICE (34% in TU500 and 73% in

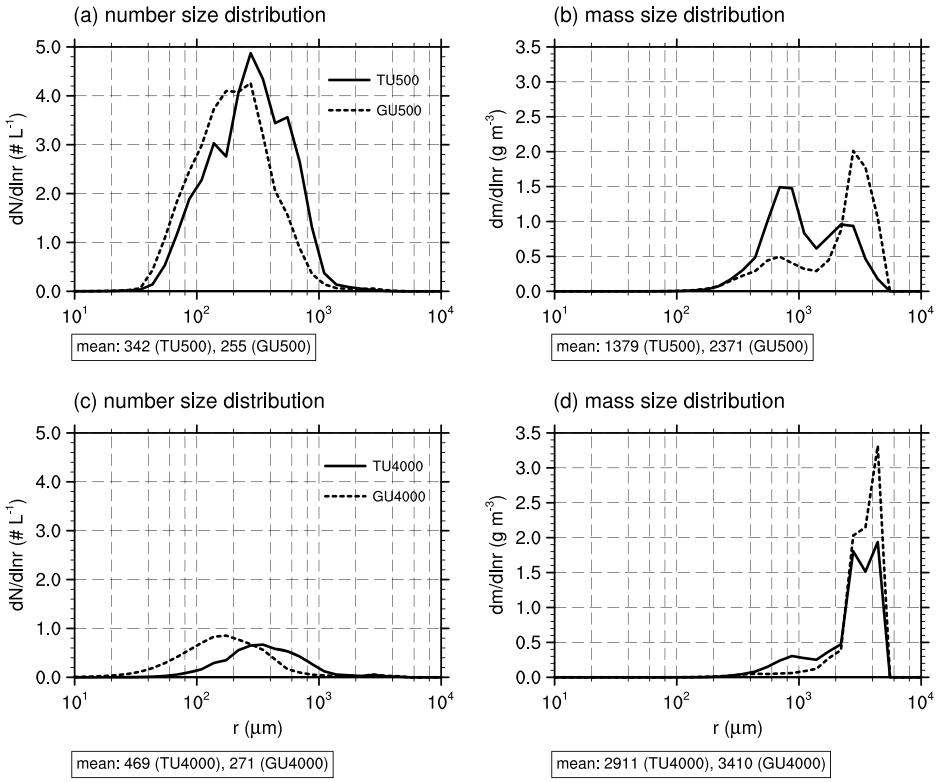

Figure 7. (a) Number size distributions and (b) mass size distributions of graupel particles averaged over the cloud core area (marked with the rectangular box in Figure 4) for $t = 130–150$ min in TU500 and GU500. (c and d) The same as Figures 7a and 7b, but for TU4000 and GU4000. The number- or mass-averaged mean radius of the graupel particles is given in each figure.

TU4000). However, in the mass size distribution, almost all graupel mass is concentrated in large graupel particles, and this feature is more pronounced under the high CCN concentration than under the low CCN concentration. Due to TICE, although the number-averaged mean radius of graupel particles increases, the mass-averaged mean radius of graupel particles decreases (42% in TU500 and 15% in TU4000). The total mass of very large graupel particles (whose radii are larger than 2 mm) decreases significantly when TICE is considered. This means that when TICE is not considered, a very small number of large graupel particles account for almost all the total graupel mass. However, when TICE is considered, small graupel particles also account for some of the total graupel mass. The decrease in the mass-averaged mean radius of graupel particles is more marked under the low CCN concentration. This is because the supersaturation is higher for the low CCN concentration, so the increase in the number of small graupel particles due to TICE is greater.

Small graupel particles do not have enough terminal velocities to penetrate the strong updraft zone in the cloud, so they tend to remain aloft and to be advected by outflow winds. On the other hand, large graupel particles have large terminal velocities, so they can fall toward the ground. The broader spatial distribution of graupel mass in the high altitudes and the decrease in graupel mass in the low altitudes in the cases with TICE are consistent with the reduction in the number of large graupel particles. Because TICE accelerates drop-drop collisions via enhanced coalescence, the droplet number concentration decreases and the supersaturation increases. This makes ice crystals grow quickly by deposition and collide with supercooled drops efficiently, which results in the enhanced formation of small graupel particles via collection of small ice crystals by large drops, as proposed in *Khain et al.* [2011]. The rapid transition from ice crystals to small graupel particles is also reflected as the decrease in ice crystal mass, depicted in Figures 4 and 5.

Figure 8 shows the vertical profiles of vertical flux of graupel mass, mass-averaged graupel terminal velocity, and vertical wind velocity averaged for $t = 130–150$ min in TU500, GU500, TU4000, and GU4000. The

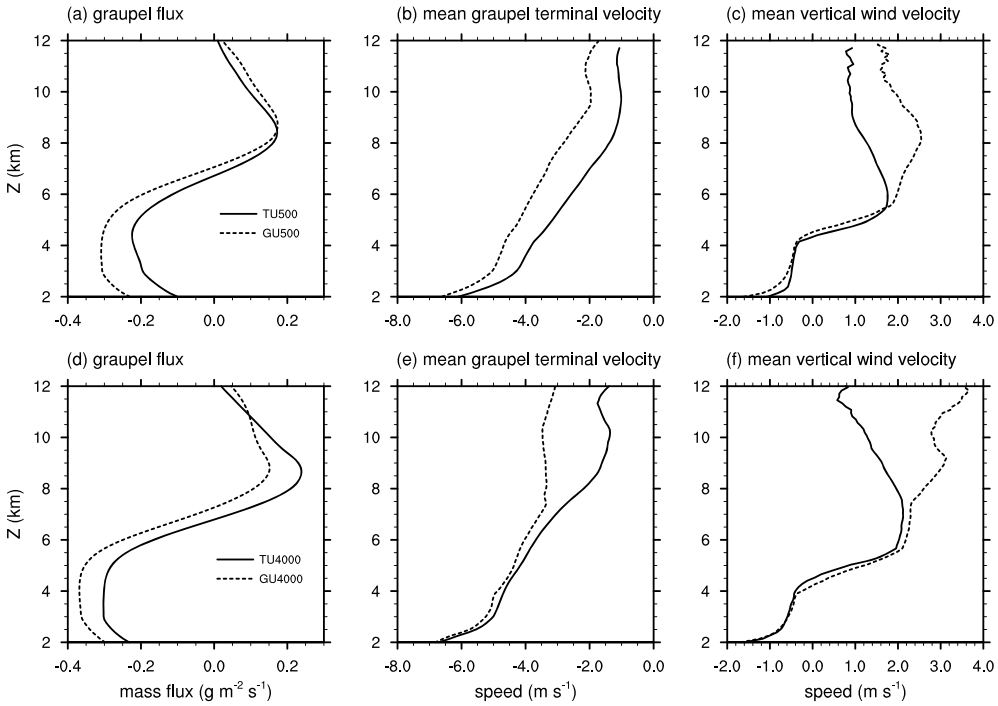

Figure 8. Vertical profiles of (a) vertical flux of graupel mass, (b) mass-averaged mean terminal velocity of graupel particles, and (c) vertical wind velocity averaged for $t = 130–150$ min in TU500 and GU500. The terminal velocity and the vertical wind velocity are averaged over the region where the graupel mass is larger than 0.1 g m^{-3}. (d–f) The same as Figures 8a–8c, but for TU4000 and GU4000. Positive and negative values mean upward and downward, respectively.

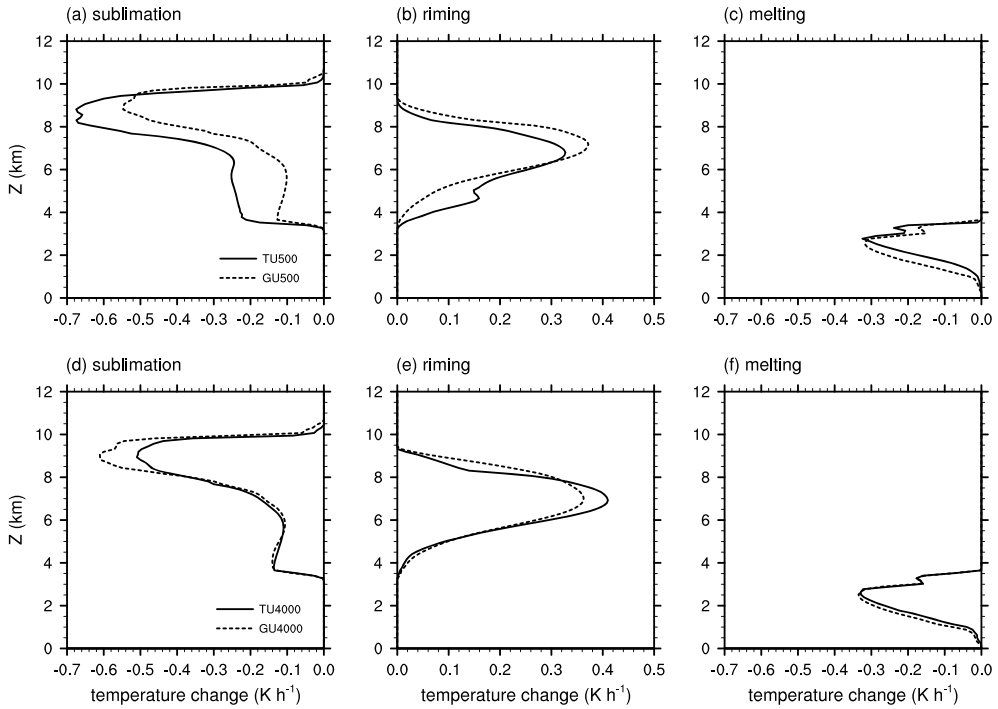

Figure 9. Vertical profiles of temperature change rate due to the latent heat from (a) sublimation, (b) riming, and (c) melting averaged over the domain for $t = 130–150$ min in TU500 and GU500. (d–f) The same as Figures 9a–9c, but for TU4000 and GU4000.

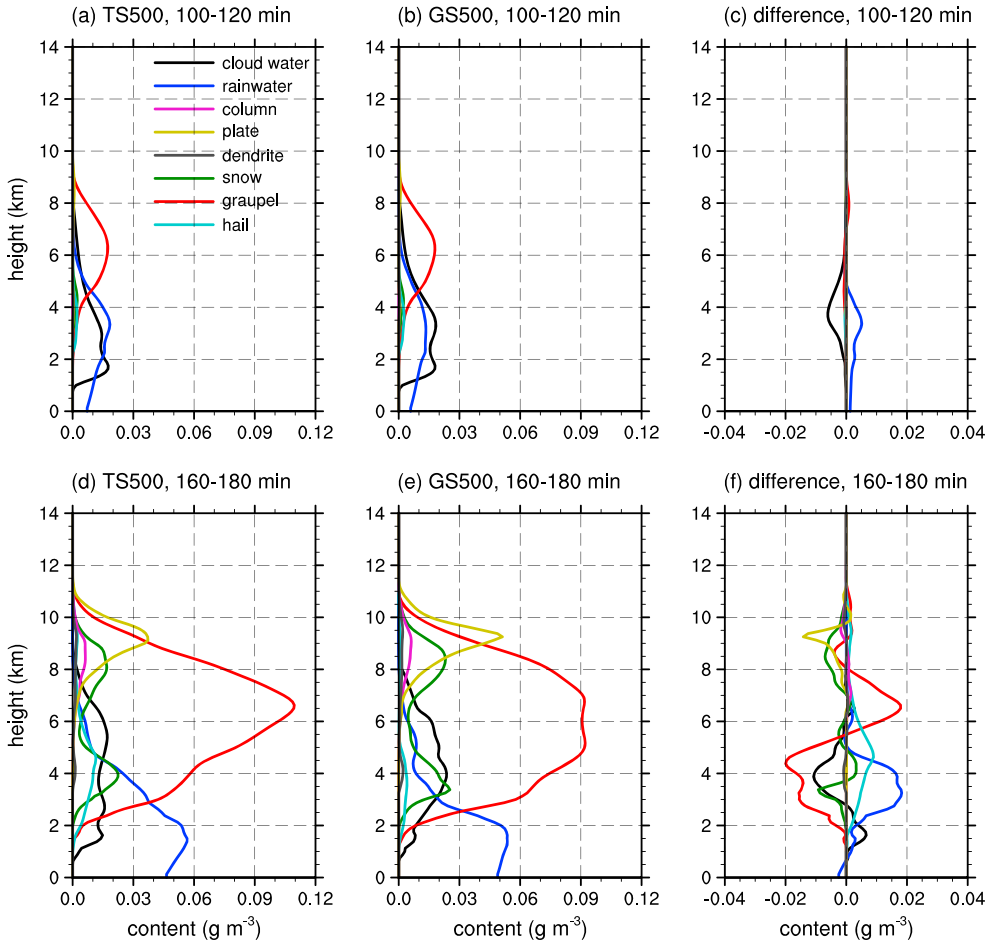

Figure 10. Vertical distribution of horizontally averaged mass of each hydrometeor type averaged for $t = 100–120$ min in (a) TS500 and (b) GS500. (c) The difference between Figure 10a and 10b. (d–f) The same as Figures 10a–10c, but averaged for $t = 160–180$ min.

vertical flux of graupel mass is affected by graupel terminal velocity, vertical wind velocity, and graupel mass. In all cases, the averaged vertical wind velocity is negative (toward the ground) in the layer $z < 4.5$ km. Also, the vertical flux of graupel mass is downward in the layer $z < 7$ km, and TICE decreases the downward flux of graupel mass. It is seen that the difference in vertical wind velocity in the lower layer between the cases with and without TICE is small, so it can make little difference in vertical flux of graupel mass. In TU500 and GU500, the large decrease in mass-averaged mean radius of graupel particles due to TICE (Figure 7b) results in a decrease in terminal velocity of graupel particle and thus the decrease in downward flux of graupel mass. In TU4000 and GU4000, however, the decrease in mass-averaged mean terminal velocity due to TICE is comparatively small because the decrease in mass-averaged mean radius of graupel particles is small (Figure 7d).

Figure 9 shows the vertical profiles of temperature change rate due to the latent heat from sublimation, riming, and melting averaged for $t = 130–150$ min in TU500, GU500, TU4000, and GU4000. Figure 9a indicates that the sublimation of ice particles increases due to TICE for the low CCN concentration. Although an increase in ice particle mass due to riming is also seen in Figure 9b, the decrease in ice particle mass due to sublimation is larger than the increase in ice particle mass due to riming. However, such an increase in sublimation is not seen for the high CCN concentration (Figure 9d). Therefore, the decrease in graupel mass in the low altitudes when TICE is considered is more likely to come from the decrease in downward flux of graupel mass, rather than from the increase in sublimation. The melting of ice particles decreases due to TICE regardless of the CCN concentration.

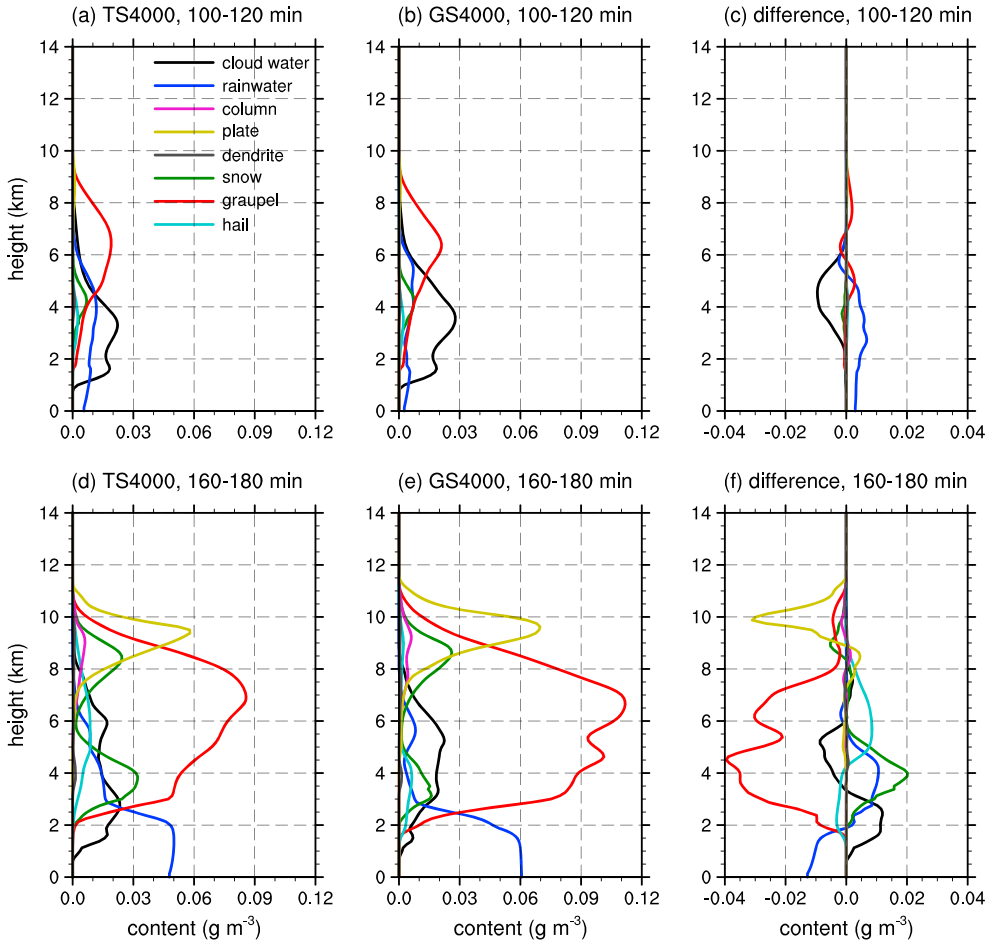

Figure 11. The same as Figure 10, but for TS4000 and GS4000.

According to *Benmoshe and Khain* [2014], TICE increases the mass and size of graupel particles in the developing and mature stage of clouds because the number of large drops increases due to TICE and the collection of small ice crystals by large drops is enhanced, whereas TICE decreases the total mass of graupel particles in the decaying stage because the riming process is enhanced in the cases without TICE due to the droplets aloft. In this study, although the domain sum of graupel mass also increases due to TICE in the developing and mature stage (not shown), the number of large graupel particles decreases due to TICE, which is opposite to the results of *Benmoshe and Khain* [2014].

To reconcile the two results, it is hypothesized that the temperature in the upper layer ($z > 8$ km) is important. The temperature in the upper layer is much lower (approximately 10°C lower) in this study than in *Benmoshe and Khain* [2014]. At first, this lower temperature in the upper layer destabilizes the cloud layer, so additional latent heat release due to the collection of small ice crystals by large drops does not affect greatly the vertical motion (Figure 3). Moreover, this lower temperature induces a larger number of ice crystals by a few times [e.g., *Meyers et al.*, 1992; *DeMott et al.*, 2010]. If the number of ice crystals is small, those ice crystals easily grow larger regardless of TICE. Hence, their growth into graupel particles can be controlled by drops. However, if the number of ice crystals is large, their further growth is suppressed. Therefore, an increase in supersaturation in the upper layer, which induces the growth of ice crystals in size, can control the growth of ice crystals into graupel particles. However, the explanation above should be regarded as a proposition. More careful studies are needed to clarify the effects of TICE on the cloud evolution.

3.3. Microphysical Structures in the Sheared Basic-State Wind Cases

Analyses similar to those for the uniform basic-state wind cases are conducted for the sheared basic-state wind cases. The vertical distribution of temporally and horizontally averaged mass of each hydrometeor

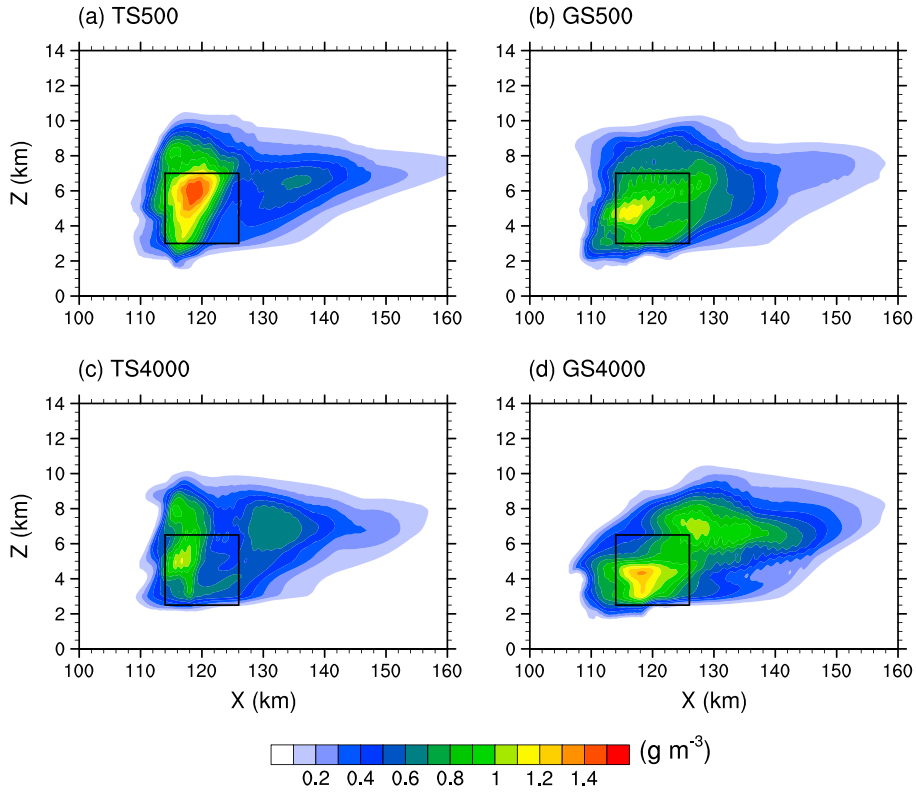

Figure 12. Graupel mass fields averaged for $t = 160–180$ min in (a) TS500, (b) GS500, (c) TS4000, and (d) GS4000. The rectangular box indicates the cloud core area.

type for the sheared basic-state wind cases are shown in Figures 10 and 11. The important features induced by TICE also appear in the sheared basic-state wind cases. TICE accelerates collisions between small droplets, so cloud water mass decreases and rainwater mass increases in the early stage ($t = 100–120$ min). For $t = 160–180$ min, as that in the uniform basic-state wind cases, graupel particles comprise a large portion of clouds, followed by rainwater and plate-type ice crystals. By comparing TS500 to GS500, it is seen that graupel mass in the layer $z > 5.5$ km increases, but graupel mass in the layer $z < 5.5$ km decreases (Figure 10f). The decrease in graupel mass appears differently in TS4000 and GS4000: graupel mass reduces in the entire layer by TICE (Figure 11f). A decrease in rainwater mass in the layer $z <$ ~1 km is seen under both the low and the high CCN concentration.

There are some noticeable differences in the distribution compared to that in the uniform basic-state wind cases. One of these is a decrease in ice crystal mass near the cloud top and resultant decrease in cloud top height. Strong vertical wind shear enhances mixing of the cloud with the surrounding dry air. Updraft velocity weakens and the amounts of cloud water and water vapor decrease by the enhanced mixing in the early stage of cloud development. Therefore, the growth of ice crystals in the high altitudes slows. Moreover, snow mass is not negligible in the sheared basic-state wind cases. Strong wind shear can advect small droplets to unsaturated areas, so the droplets are more likely to evaporate. This decrease in cloud droplets (Figures 10 and 11 compared to Figures 4 and 5) gives rise to the lack of necessary sources for growing ice crystals into ice particles with relatively high densities via riming. Thus, graupel mass decreases, whereas snow mass increases.

The graupel mass field averaged for $t = 160–180$ min in TS500, GS500, TS4000, and GS4000 are shown in Figure 12. Comparing to the graupel mass field in the uniform basic-state wind cases, graupel mass in the cloud core area decreases by about half, and graupel particles spread across a far wider area. Although Figures 10f and 9f also show a decrease in graupel mass due to TICE in the low altitudes, distribution patterns are different: the narrow shaft area that is seen in the uniform basic-state wind cases (Figures 6b and 6d) does not appear in Figures 12b and 12d. Rather, graupel mass in the cloud core area is distributed more uniformly when TICE is not considered.

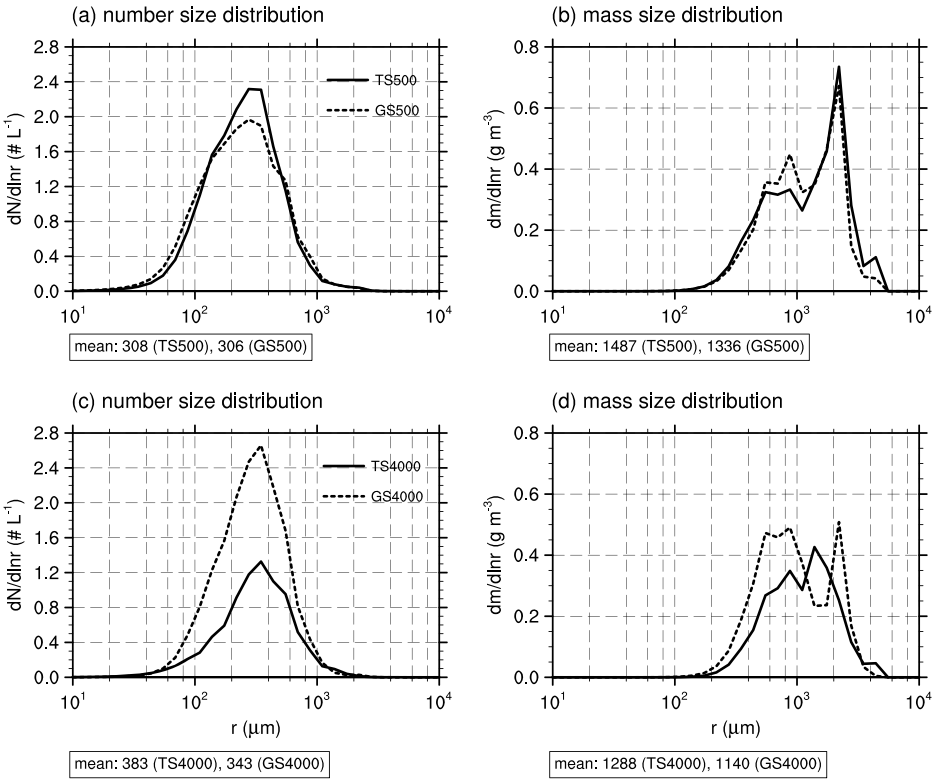

Figure 13. (a) Number size distributions and (b) mass size distributions of graupel particles averaged over the cloud core area (marked with the rectangular box in Figure 10) for $t = 160–180$ min in TS500 and GS500. (c and d) The same as Figures 13a and 13b, but for TS4000 and GS4000. The number- or mass-averaged mean radius of the graupel particles is given in each figure.

The number and mass size distributions of graupel particles in the cloud core area in TS500, GS500, TS4000, and GS4000 are plotted in Figure 13. This figure shows some features that are different from those in the uniform basic-state wind cases. In the number size distribution, the range of the radii of graupel particles is almost the same and it is only the concentration that changes due to TICE, whereas a shift is seen in the uniform basic-state wind cases. In the mass size distribution, the mass-averaged mean radius of graupel particles increases slightly when TICE is considered. This is opposite to the behavior in the uniform basic-state wind cases. The difference in the mass size distributions between the cases with and without TICE is very small. In the uniform basic-state wind cases, the faster growth of ice crystals into small graupel particles due to TICE is the key to the differences in the number and mass size distributions of graupel particles. In the sheared basic-state wind cases, however, the number of ice crystals is much smaller than in the uniform basic-state wind cases, so the size distributions in the cases with and without TICE show little difference.

Figure 14 shows the vertical profiles of vertical flux of graupel mass, mass-averaged mean terminal velocity of graupel particles, and vertical wind velocity averaged for $t = 160–180$ min in TS500, GS500, TS4000, and GS4000. The overall difference in downward flux of graupel mass in the lower layer between the cases with and without TICE is small compared to that in the uniform basic-state wind cases. Comparing TS500 to GS500, a small decrease in mass-averaged mean terminal velocity of graupel particles is seen. However, this would be cancelled out by the enhanced downdraft. Similar to the uniform basic-state wind cases, the difference in mean terminal velocity between the cases with and without TICE is smaller under the high CCN concentration than under the low CCN concentration. The mean terminal velocities of graupel particles in TS4000 and GS4000 are very similar. The decrease in vertical flux of graupel mass might come from the decrease in graupel mass (Figure 11).

Figure 15 shows the vertical profiles of temperature change rate due to the latent heat from sublimation, riming, and melting averaged for $t = 160–180$ min in TS500, GS500, TS4000, and GS4000. The most

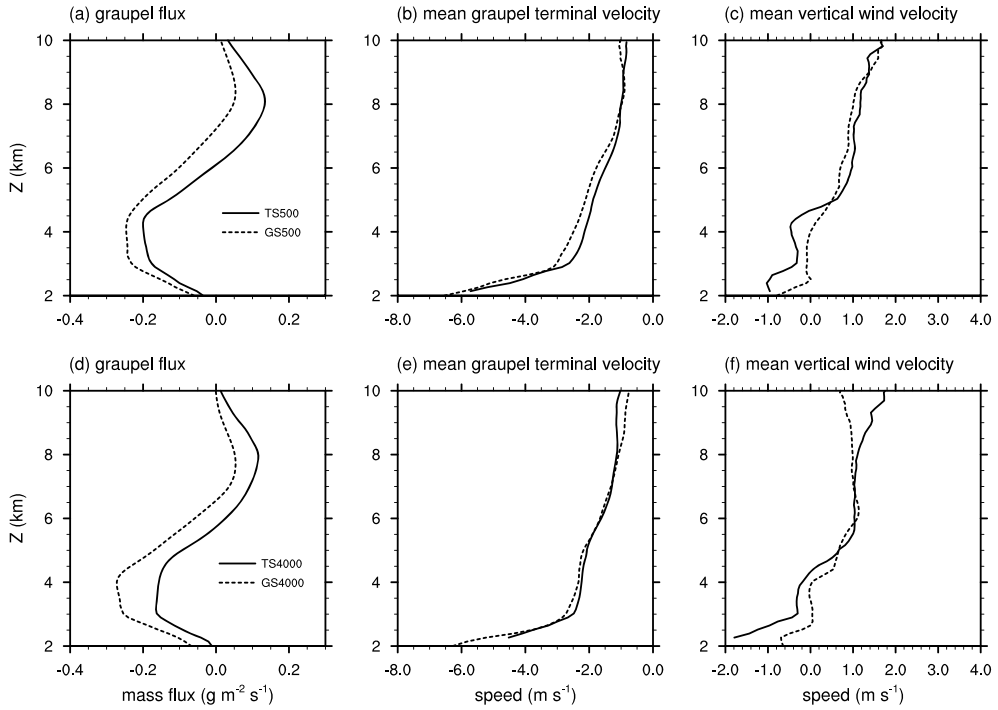

Figure 14. Vertical profiles of (a) vertical flux of the graupel mass, (b) mass-averaged mean terminal velocity of graupel particles, and (c) vertical wind velocity averaged for $t = 160–180$ min in TS500 and GS500. The terminal velocity and the vertical wind velocity are averaged over the region where the graupel mass is larger than 0.1 g m^{-3}. (d–f) The same as Figures 14a–14c, but for TS4000 and GS4000. Positive and negative values mean upward and downward, respectively.

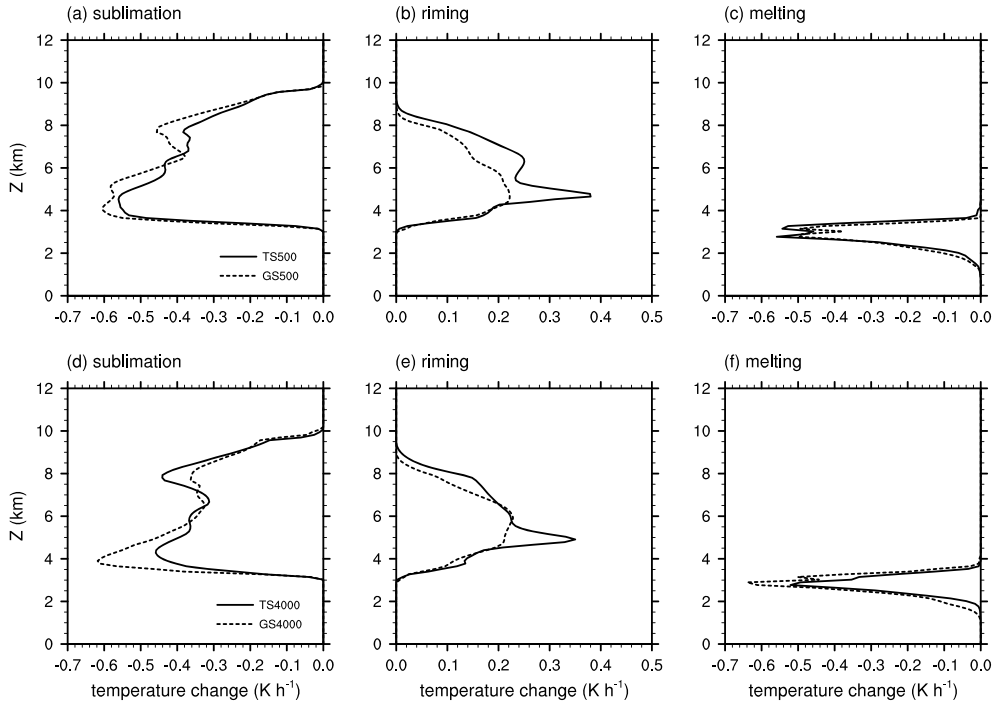

Figure 15. Vertical profiles of temperature change rate due to the latent heat from (a) sublimation, (b) riming, and (c) melting averaged over the domain for $t = 160–180$ min in TS500 and GS500. (d–f) The same as Figures 15a–15c, but for TS4000 and GS4000.

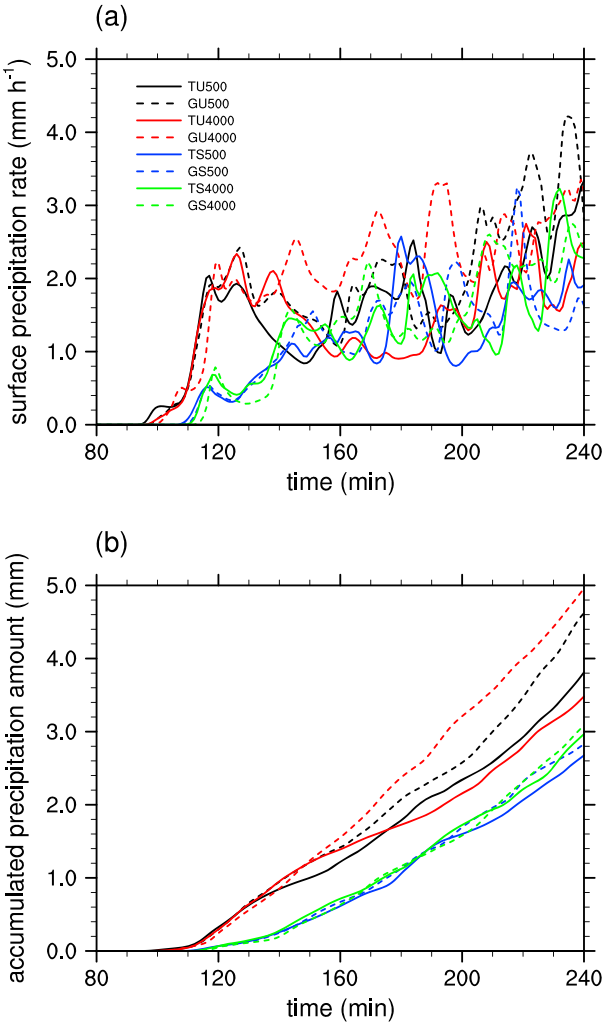

Figure 16. (a) Surface precipitation rate and (b) accumulated surface precipitation time series averaged over the domain in all simulation cases.

striking difference compared to that in the uniform basic-state wind cases is an increase in sublimation of ice particles in the layer 4 km $< z <$ 6 km. In this layer, ice sublimation in the sheared basic-state wind cases increases more than two times than that in the uniform basic-state wind cases. Strong wind shear makes more ice particles fall into unsaturated areas. Increased ice sublimation compared to that in the uniform basic-state wind cases is seen in all the periods of the numerical simulations, not only for t = 160–180 min.

3.4. Surface Precipitation

Time series for the surface precipitation rate and the amount of accumulated surface precipitation in all simulation cases are depicted in Figure 16. Surface precipitation is strongly affected by the vertical wind shear. The amount of accumulated surface precipitation in the sheared basic-state wind cases reduces by about 35% compared to that in the uniform basic-state wind cases, which is expected to be the result of the increased ice sublimation (Figures 15a and 15d).

In previous studies [e.g., *Seifert et al.*, 2010; *Benmoshe et al.*, 2012; *Wyszogrodzki et al.*, 2013], the zones with high turbulent dissipation rates and the zones with large cloud number concentrations tend to be collocated, particularly near the cloud top in the early cloud development stage. This collocation helps turbulence efficiently accelerate the formation of first raindrop and induce an increase in surface precipitation in warm

clouds. Like the results of those studies, such collocation also occurs in this study (Figure 2) and surface precipitation starts about 5 min earlier and increases during the warm rain stage (first 5–10 min of surface precipitation) due to TICE in all cases of this study.

In spite of the accelerated onset of surface precipitation, however, the amount of accumulated surface precipitation decreases due to TICE in all cases. For example, the amount of accumulated surface precipitation decreases by 18% in TU500 compared to GU500 during the simulation period. This result largely agrees with the result of *Benmoshe et al.* [2012] in which the amount of surface precipitation always decreases regardless of aerosol concentrations. The decrease in the amount of surface precipitation is larger in the uniform basic-state wind cases than in the sheared basic-state wind cases. This is mainly because of the changes in the size distributions of graupel particles. This is examined in section 3.2. In the uniform basic-state wind cases, the decrease in the amount of surface precipitation is larger for the high CCN concentration than for the low CCN concentration. Although the decrease is also seen in the sheared basic-state wind cases, it is so small that the comparison between the low and the high CCN concentration case seems unnecessary. Note that in the uniform basic-state wind cases, the amount of accumulated surface precipitation over the simulation period increases with increasing CCN concentration when TICE is not considered, whereas the opposite trend appears when TICE is considered.

4. Summary and Conclusions

The effects of turbulence-induced collision enhancement (TICE) on mixed-phase deep convective clouds were investigated using a 2-D bin microphysics cloud model. This study considered TICE for drop-drop collisions and drop-graupel collisions. TICE is determined by the turbulence dissipation rate and the Taylor microscale Reynolds number, which are calculated using the turbulent kinetic energy. Two types of basic-state winds and two aerosol concentrations were considered to examine the effects of TICE with different basic-state winds and aerosol concentrations. Despite somewhat coarser grid size, the simulated turbulence dissipation rates fall within a range similar to those of previous studies using finer grid sizes.

TICE accelerates coalescence between droplets in the early cloud development stage. The number of droplets decreases due to the accelerated collisions. This causes an increase in supersaturation in the high altitudes. Ice crystals grow more quickly by deposition due to the increased supersaturation, collide with supercooled drops more efficiently, and hence grow to the small graupel particles more easily via the collection of ice crystals by drops. Therefore, in the cases that consider TICE, graupel particles with small sizes are relatively large in number and account for some of the total graupel mass in the cloud core area. On the other hand, in the cases that do not consider TICE, graupel particles with large sizes account for almost all the total graupel mass. Graupel particles with small sizes have slower terminal velocities than those with large sizes. Thus, graupel particles in the high altitudes are distributed across a wider area, and the downward flux of graupel mass decreases when TICE is considered. This induces a decrease in surface precipitation due to the decreased melting of graupel particles. The increased sublimation of ice particles due to TICE also decreases the amount of surface precipitation, despite its limited role. The effects of TICE in the sheared basic-state wind cases are comparatively small. This is because strong wind shear diminishes cloud development in the early stage, so the number of ice crystals, which is the key to the difference by TICE, decreases significantly. The results of this study largely agree with those of previous study [e.g., *Benmoshe and Khain*, 2014]: the domain sum of graupel mass increases due to TICE particularly in the developing and mature stage of cloud development, and the surface precipitation always decreases in the cases with TICE. However, some parts of the results of this study are somewhat different from those of *Benmoshe and Khain* [2014]. It is hypothesized that the difference in upper air temperature might cause the differences in the results. More careful studies are needed to clarify the effects of TICE on the evolution of mixed-phase deep convective clouds.

Although recent individual studies show similar TICE for collisions between droplets, some discrepancies still remain [*Grabowski and Wang*, 2013]. Moreover, there exists a significant lack of knowledge about TICE for collisions that include ice particles. The effects of turbulence on collisions between cloud particles need to be investigated further. Beside the collision process, the effects of turbulence on cloud microphysical processes should also be considered more carefully. For example, the effects of turbulence on diffusional processes can broaden the size distribution of droplets [e.g., *Lanotte et al.*, 2009; *Korolev et al.*, 2013]. Mixing

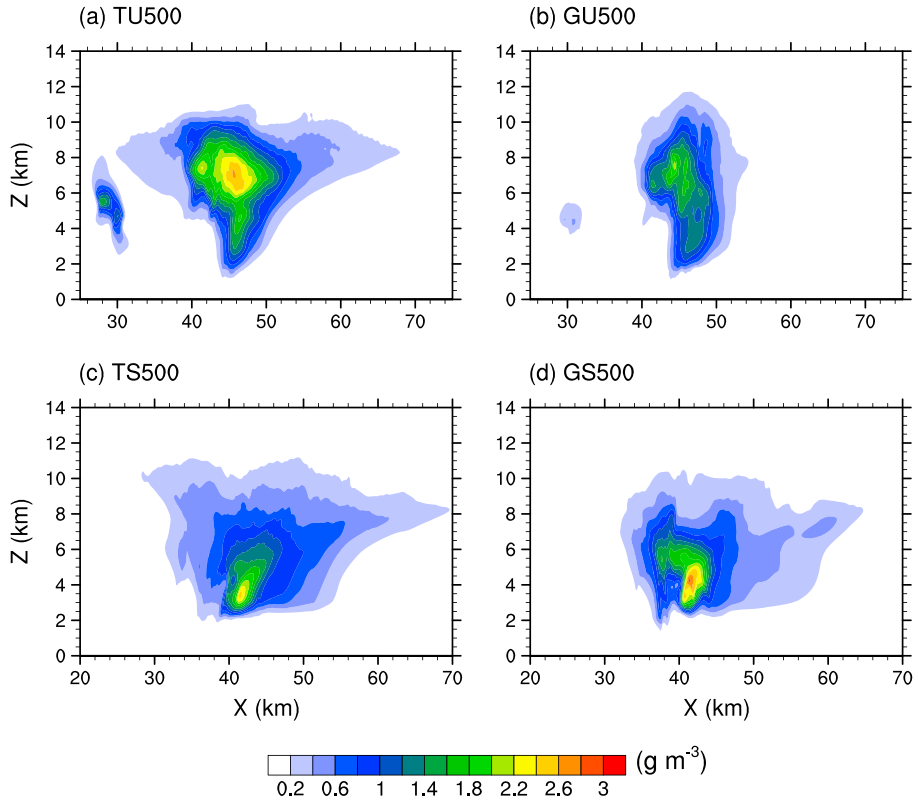

Figure A1. Graupel mass fields in (a) TU500, (b) GU500, (c) TS500, and (d) GS500 with the horizontal grid size of 125 m. Figures A1a and A1b are averaged for $t = 130–150$ min and Figures A1c and A1d for $t = 160–180$ min.

process can also affect cloud water content and the size distribution of droplets [e.g., *Gerber et al.*, 2008]. Further investigations into the effects of turbulence on cloud microphysical processes would lead to a better understanding of clouds and precipitation.

Appendix A: Sensitivity Tests for Horizontal Grid Size

To show that the horizontal grid size used in this study ($\Delta x = 250$ m) does not have a significant impact on the simulation results, four additional sensitivity experiments are conducted with a finer grid size. The horizontal grid size of the experiments is 125 m, and the horizontal domain size is also reduced by half. In the sheared basic-state wind cases, a uniform wind of -12 m s^{-1} is imposed into the original sheared basic-state wind for simulated clouds to be confined to the reduced computational domain. CCN concentration N_0 is 500 cm^{-3} in all of the sensitivity experiments.

Figure A1 shows the graupel mass fields averaged for $t = 130–150$ min in the sensitivity tests for TU500 and GU500 and averaged for $t = 160–180$ min in the sensitivity tests for TS500 and GS500. Compared to Figures 6a, 6b, 12a, and 12b, although the cloud structures tend to be smooth with larger grid size, the most important features are evident. In the case with TICE, graupel particles spread out across a wider area, but the mass of graupel particles is smaller in the lower layer. Figure A2 shows the vertical distribution of horizontally averaged mass of each hydrometeor type averaged for $t = 130–150$ min in TU500 and GU500 and averaged for $t = 160–180$ min in TU500 and GU500. Figure A2 also support the simulation results with $\Delta x = 250$ m (see Figures 4d–4f and 10d–10f).

In surface precipitation, although precipitation tendency in TS500 and GS500 for $t = 160–180$ min is opposite to that of the original simulations, accumulated surface precipitation also always decreases due to TICE (not shown). The difference in surface precipitation induced by TICE reduces in the sensitivity experiments. The similar result has also been reported in *Seifert et al.* [2010]. Further careful studies are needed to investigate the effects of TICE on surface precipitation of mixed-phase deep convective clouds.

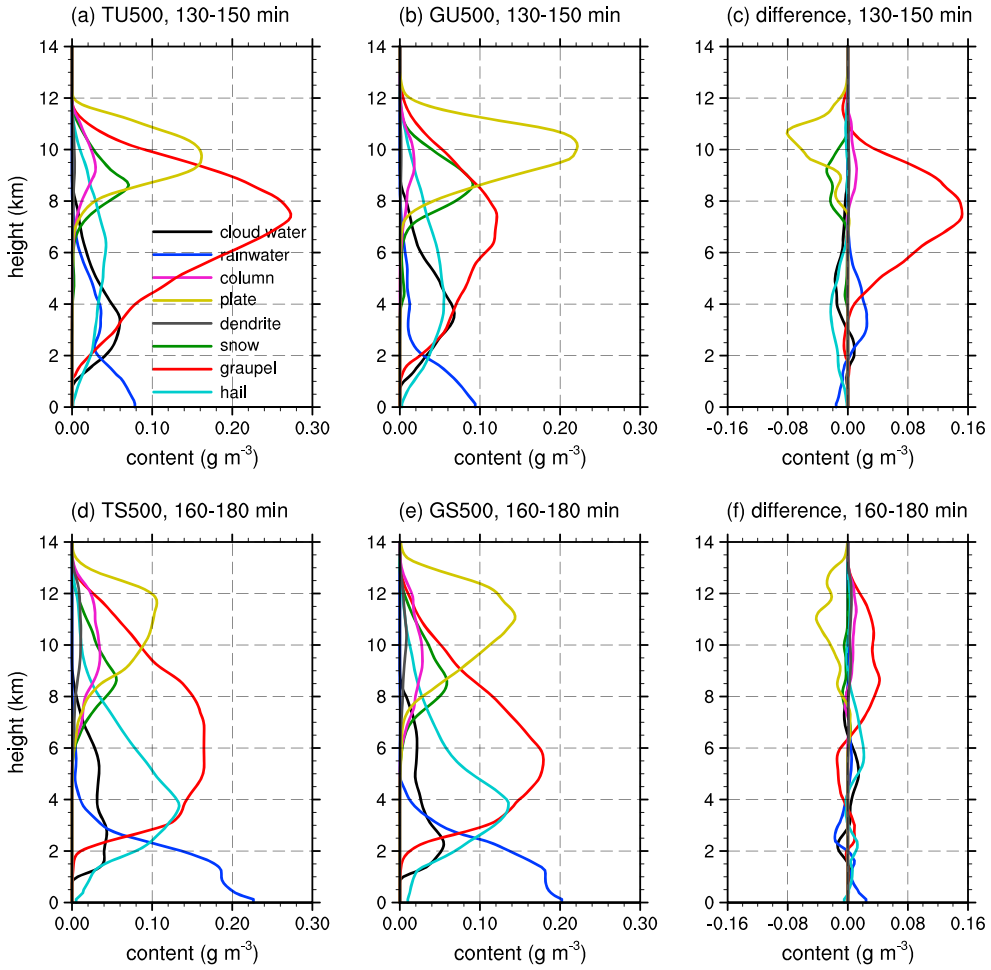

Figure A2. Vertical distribution of horizontally averaged mass of each hydrometeor type averaged for $t = 130–150$ min in (a) TU500 and (b) GU500 with the horizontal grid size of 125 m. (c) The difference between Figures A2a and A2b. (d–f) The same as Figures A2a–A2c, but averaged for $t = 160–180$ min in (d) TS500 and (e) GS500 with the horizontal grid size of 125 m.

Acknowledgments

The authors are grateful to three anonymous reviewers for providing valuable comments on this work. The cloud model used in this study was provided by Alexander Khain of The Hebrew University of Jerusalem, Israel. All data of this study are accessible via personal communication with the corresponding author (jjbaik@snu.ac.kr). The first and second authors were supported by the Korea Meteorological Administration Research and Development Program under grant CATER 2012-6030 and also by the National Research Foundation of Korea (NRF) grant funded by the Korea Ministry of Science, ICT and Future Planning (MSIP) (2011-0017041). The third author was supported by the R&D project on the development of Korea's global numerical weather prediction systems of Korea Institute of Atmospheric Prediction Systems (KIAPS) funded by the Korea Meteorological Administration (KMA). The authors thank supercomputer management division of the Korea Meteorological Administration for providing us with the supercomputer resource and consulting on technical support.

References

Ayala, O., B. Rosa, and L.-P. Wang (2008), Effects of turbulence on the geometric collision rate of sedimenting droplets. Part 2. Theory and parameterization, *New J. Phys.*, *10*, 075016, doi:10.1088/1367-2630/10/7/075016.

Benmoshe, N., and A. P. Khain (2014), The effects of turbulence on the microphysics of mixed-phase deep convective clouds investigated with a 2-D cloud model with spectral bin microphysics, *J. Geophys. Res. Atmos.*, *119*, 207–221, doi:10.1002/2013JD020118.

Benmoshe, N., M. Pinsky, A. Pokrovsky, and A. Khain (2012), Turbulent effects on the microphysics and initiation of warm rain in deep convective clouds: 2-D simulations by a spectral mixed-phase microphysics cloud model, *J. Geophys. Res.*, *117*, D06220, doi:10.1029/2011JD016603.

Bigg, E. K. (1953), The formation of atmospheric ice crystals by the freezing of droplets, *Q. J. R. Meteorol. Soc.*, *79*, 510–519.

Carrió, G. G., and W. R. Cotton (2011), Urban growth and aerosol effects on convection over Houston. Part II: Dependence of aerosol effects on instability, *Atmos. Res.*, *102*, 167–174.

Carrió, G. G., W. R. Cotton, and W. Y. Y. Cheng (2010), Urban growth and aerosol effects on convection over Houston. Part I: The August 2000 case, *Atmos. Res.*, *96*, 560–574.

DeMott, P. J., A. J. Prenni, X. Liu, S. M. Kreidenweis, M. D. Petters, C. H. Twohy, M. S. Richardson, T. Eidhammer, and D. C. Rogers (2010), Predicting global atmospheric ice nuclei distributions and their impacts on climate, *Proc. Natl. Acad. Sci. U.S.A.*, *107*, 11,217–11,222.

Devenish, B. J., et al. (2012), Droplet growth in warm turbulent clouds, *Q. J. R. Meteorol. Soc.*, *138*, 1401–1429.

Fan, J., T. Yuan, J. M. Comstock, S. Ghan, A. Khain, L. R. Leung, Z. Li, V. J. Martins, and M. Ovchinnikov (2009), Dominant role by vertical wind shear in regulating aerosol effects on deep convective clouds, *J. Geophys. Res.*, *114*, D22206, doi:10.1029/2009JD012352.

Franklin, C. N. (2008), A warm rain microphysics parameterization that includes the effect of turbulence, *J. Atmos. Sci.*, *65*, 1795–1816.

Franklin, C. N., P. A. Vaillancourt, M. K. Yau, and P. Bartello (2005), Collision rates of cloud droplets in turbulent flows, *J. Atmos. Sci.*, *62*, 2451–2466.

Gerber, H. E., G. M. Frick, J. B. Jensen, and J. G. Hudson (2008), Entrainment, mixing, and microphysics in trade-wind cumulus, *J. Meteorol. Soc. Jpn.*, *86A*, 87–106.

Grabowski, W. W., and L.-P. Wang (2013), Growth of cloud droplets in a turbulent environment, *Annu. Rev. Fluid Mech.*, *45*, 293–324.
Hallett, J., and S. C. Mossop (1974), Production of secondary ice crystals during the riming process, *Nature*, *249*, 26–28.
Han, J.-Y., and J.-J. Baik (2010), Theoretical studies of convectively forced mesoscale flows in three dimensions. Part II: Shear flow with a critical level, *J. Atmos. Sci.*, *67*, 694–712.
Han, J.-Y., J.-J. Baik, and A. P. Khain (2012), A numerical study of urban aerosol impacts on clouds and precipitation, *J. Atmos. Sci.*, *69*, 504–520.
Khain, A., M. Ovtchinnikov, M. Pinsky, A. Pokrovsky, and H. Krugliak (2000), Notes on the state-of-the-art numerical modeling of cloud microphysics, *Atmos. Res.*, *55*, 159–224.
Khain, A., M. Pinsky, T. Elperin, N. Kleeorin, I. Rogachevskii, and A. Kostinski (2007), Critical comments to results of investigations of drop collisions in turbulent clouds, *Atmos. Res.*, *86*, 1–20.
Khain, A., D. Rosenfeld, A. Pokrovsky, U. Blahak, and A. Ryzhkov (2011), The role of CCN in precipitation and hail in a mid-latitude storm as seen in simulations using a spectral (bin) microphysics model in a 2D dynamic frame, *Atmos. Res.*, *99*, 129–146.
Köhler, H. (1936), The nucleus in and the growth of hygroscopic droplets, *Trans. Faraday Soc.*, *32*, 1152–1161.
Korolev, A., M. Pinsky, and A. Khain (2013), A new mechanism of droplet size distribution broadening during diffusional growth, *J. Atmos. Sci.*, *70*, 2051–2071.
Kunnen, R. P. J., C. Siewert, M. Meinke, W. Schröder, and K. D. Beheng (2013), Numerically determined geometric collision kernels in spatially evolving isotropic turbulence relevant for droplets in clouds, *Atmos. Res.*, *127*, 8–21.
Lanotte, A. S., A. Seminara, and F. Toschi (2009), Cloud droplet growth by condensation in homogeneous isotropic turbulence, *J. Atmos. Sci.*, *66*, 1685–1697.
Lee, S. S., and G. Feingold (2013), Aerosol effects on the cloud-field properties of tropical convective clouds, *Atmos. Chem. Phys.*, *13*, 6713–6726.
Lee, S. S., L. J. Donner, and J. E. Penner (2010), Thunderstorm and stratocumulus: How does their contrasting morphology affect their interactions with aerosols?, *Atmos. Chem. Phys.*, *10*, 6819–6837.
Meyers, M. P., P. J. DeMott, and W. R. Cotton (1992), New primary ice-nucleation parameterizations in an explicit cloud model, *J. Appl. Meteorol.*, *31*, 708–721.
Pinsky, M., A. Khain, D. Rosenfeld, and A. Pokrovsky (1998), Comparison of collision velocity differences of drops and graupel particles in a very turbulent cloud, *Atmos. Res.*, *49*, 99–113.
Pinsky, M., A. Khain, and H. Krugliak (2008), Collisions of cloud droplets in a turbulent flow. Part V: Application of detailed tables of turbulent collision rate enhancement to simulation of droplet spectra evolution, *J. Atmos. Sci.*, *65*, 357–374.
Pinsky, M. B., and A. P. Khain (1998), Some effects of cloud turbulence on water–ice and ice–ice collisions, *Atmos. Res.*, *47–48*, 69–86.
Riechelmann, T., Y. Noh, and S. Raasch (2012), A new method for large-eddy simulations of clouds with Lagrangian droplets including the effects of turbulent collision, *New J. Phys.*, *14*, 065008, doi:10.1088/1367-2630/14/6/065008.
Rosenfeld, D., U. Lohmann, G. B. Raga, C. D. O'Dowd, M. Kulmala, S. Fuzzi, A. Reissell, and M. O. Andreae (2008), Flood or drought: How do aerosols affect precipitation?, *Science, 321*, 1309–1313.
Rotunno, R., J. B. Klemp, and M. L. Weisman (1988), A theory for strong, long-lived squall lines, *J. Atmos. Sci.*, *45*, 463–485.
Seifert, A., and K. Beheng (2006), A two-moment cloud microphysics parameterization for mixed-phase clouds. Part II: Maritime vs. continental deep convective storms, *Meteorol. Atmos. Phys.*, *92*, 67–82.
Seifert, A., L. Nuijens, and B. Stevens (2010), Turbulence effects on warm-rain autoconversion in precipitating shallow convection, *Q. J. R. Meteorol. Soc.*, *136*, 1753–1762.
Siebert, H., K. Lehmann, and M. Wendisch (2006), Observations of small-scale turbulence and energy dissipation rates in the cloudy boundary layer, *J. Atmos. Sci.*, *61*, 1451–1466.
Siebert, H., R. A. Shaw, and Z. Warhaft (2010), Statistics of small-scale velocity fluctuations and internal intermittency in marine stratocumulus clouds, *J. Atmos. Sci.*, *67*, 262–273.
Thorpe, A. J., M. J. Miller, and M. W. Moncrieff (1982), Two-dimensional convection in nonconstant shear: A model of midlatitude squall lines, *Q. J. R. Meteorol. Soc.*, *108*, 739–762.
Twomey, S. (1959), The nuclei of natural cloud formation. Part II: The supersaturation in natural clouds and the variation of cloud droplet concentration, *Pure Appl. Geophys.*, *43*, 243–249.
Vali, G. (1975), Remarks on the mechanism of atmospheric ice nucleation, in *Proceedings of the 8th International Conference on Nucleation*, pp. 265–269, Gidrometeoizdat, Saint Petersburg.
Weisman, M. L., and J. B. Klemp (1982), The dependence of numerically simulated convective storms on vertical wind shear and buoyancy, *Mon. Weather Rev.*, *110*, 504–520.
Wyszogrodzki, A. A., W. W. Grabowski, L.-P. Wang, and O. Ayala (2013), Turbulent collision-coalescence in maritime shallow convection, *Atmos. Chem. Phys.*, *13*, 8471–8487.
Zhou, Y., A. S. Wexler, and L.-P. Wang (2001), Modelling turbulent collision of bidisperse inertial particles, *J. Fluid Mech.*, *433*, 77–104.